AAS 22-015

LOW-THRUST TRAJECTORY OPTIMIZATION FOR THE SOLAR SYSTEM PONY EXPRESS

Alex Pascarella*†, Robyn Woollands‡§, Etienne Pellegrini¶, Marc Sanchez-Net‖, Joshua Vander Hook**

We present a method for designing and optimizing Earth-Mars cycler orbits for the Solar System Pony Express (SSPE) mission concept. The SSPE is aimed at augmenting the capabilities of the Deep Space Network (DSN) by enabling high latency and high bandwidth communications through the use of interplanetary data mules. The SSPE will leverage a network of smallsats, outfitted with optical laser communications, and by exploiting cycler orbits the SSPE will make flybys of Mars at least once a year, retrieving 1-3 petabits of data per flyby from missions already operating at the planet. This data will then be downlinked to Earth during the next Earth flyby, also occurring about once a year. The SSPE satellites are launched as a rideshare payload with another Mars-bound mission. Each courier satellite flying in the SSPE network is equipped with a low-thrust propulsion system that is used for cycler orbit injection and for targeting flybys of Earth and Mars. Cycler orbits are first computed using a patched conic approximation and impulsive thrust. These candidate solutions are then transitioned into a higher-fidelity ephemeris model, and using an indirect optimization method, fuel-optimal low-thrust transfers are computed between each pair of flybys. We present a high-fidelity candidate solution where a 500 kg courier spacecraft is inserted into an Earth-Mars cycler orbit using only 36 kg of propellant, and a further 2 kg of propellant is required to target eight subsequent flybys over a period of six years. This is very feasible from a mission design perspective and it also demonstrates that solutions obtained in the patched conics model can be successfully transitioned to the ephemeris model using low-thrust propulsion.

INTRODUCTION

Telecommunications is a fundamental aspect of space exploration. Satellites, interplanetary spacecraft, landers and rovers are crucial assets designed to acquire data and transmit it back to Earth, where thorough analysis and investigation helps further our collective knowledge of the Solar System and the Universe. Often, the impact of a scientific mission is assessed based on the amount of data it returned over its lifetime and the number of publications that made use of the data. The data volumes generated by a mission depend on several factors, such as the design of the spacecraft, the technology used for telecommunication, and the distance from Earth.

*Graduate Research Assistant, Department of Aerospace Engineering, University of Illinois at Urbana-Champaign, IL 61801.

†JPL Summer Intern, Jet Propulsion Laboratory, California Institute of Technology, CA 91109.

‡Assistant Professor, Department of Aerospace Engineering, University of Illinois at Urbana-Champaign, IL 61801.

§JPL Affiliate, Jet Propulsion Laboratory, California Institute of Technology, CA 91109.

¶Mission Design Engineer, Jet Propulsion Laboratory, California Institute of Technology, CA 91109.

‖Data Scientist, Jet Propulsion Laboratory, California Institute of Technology, CA 91109.

**Group Supervisor, Jet Propulsion Laboratory, California Institute of Technology, CA 91109.

Currently, NASA supports interplanetary spacecraft missions using the Deep Space Network (DSN). The DSN is a global radio telecommunication network composed of three ground segment facilities, spaced apart by about 120° around the Earth, and each facility operates several 34-meter antennas and one 70-meter antenna. Thanks to the strategic placement of the facilities and the large dish antennas, the DSN is able to constantly communicate with spacecraft over interplanetary distances. However, the use of radio waves and the large distances between the antenna and the probes mean that the network bandwidth is very limited, and as a result restricts the maximum data volume that a mission can return. In addition, the DSN is a resource that is shared by many missions which further reduces the data volume that can be returned by a single probe.

The Solar System Pony Express (SSPE)[1] is a mission concept that is being investigated at the Jet Propulsion Laboratory as part of the NASA Innovative Advanced Concepts (NIAC) program. The objective of the study is to augment the data transmission rates of the DSN using the idea of *data mules*. Data mules are small spacecraft that travel to a remote location (e.g. Mars) where they acquire data in close range to the probe's transmitter and then carry the data back to Earth where it is downlinked in close range to the receiver. This enables high latency and high bandwidth communication. In the case of a space network, the data transmission rates can be further increased by utilizing optical telecommunications, which allows for a larger bandwidth but also requires a strict pointing accuracy.[2]

A network of interplanetary data mules could be established by exploiting cycler orbits.[3] These are trajectories that regularly encounter two or more celestial bodies along their path and require a modest amount of propellant for navigation. For the purpose of this study we simulate a network of Earth-Mars cyclers, but the concept could be extended to Venus[4] or the outer planets.[5] In the current mission scenario, one or more smallsats could be launched as a secondary payload onboard a mission bound for Mars. After launch, the data mules use their own low-thrust propulsion system to inject into a cycler orbit and target subsequent flybys of Earth and Mars. During the Mars flybys, data is uplinked from spacecraft already operating at Mars (in orbit or on the surface) and during Earth flybys data is downlinked back to Earth.

In this paper we focus specifically on the trajectory design and optimization of Earth-Mars cycler orbits for the SSPE mission. We simulate trajectories that make use of low-thrust propulsion and include a high-fidelity model that incorporates the gravity of the Sun, Earth and Mars. Low-thrust space missions are becoming more common due to the benefits afforded by ion engines. Ion engines are more efficient than chemical engines due to their high specific impulse, and they are also much smaller/lighter which allows for the design of smaller spacecraft that can be launched economically as a secondary payload.

Two main classes of methods are used to solve for low-thrust spacecraft trajectories. The first class, direct methods, transcribes the system dynamics into a nonlinear programming problem. Generally, direct methods are robust to an initial guess, but are computationally expensive and are not guaranteed to result in an optimal solution. The second class, indirect methods, seeks to satisfy the necessary conditions for optimality. Although indirect methods ensure that the solution is at least locally optimal, they are extremely sensitive to initial guesses and convergence can be difficult. To overcome this challenge, we make use of continuation to smooth the bang-bang control in the early iterations which significantly improves convergence. The indirect method with continuation has proven to be very reliable and is the method of choice for this paper.

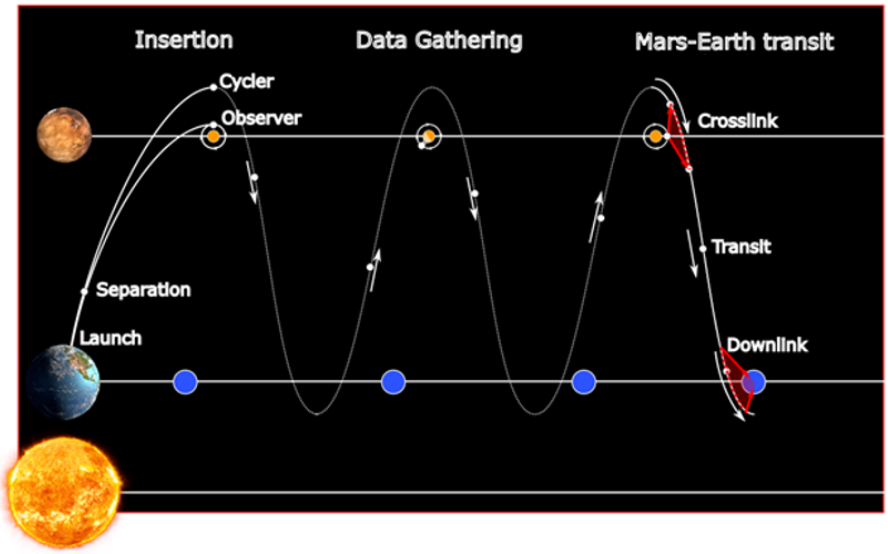

Figure 1. Concept of operations for one cycler spacecraft.

INDIRECT OPTIMAL CONTROL FORMULATION

Modified Equinoctial Elements (MEEs)[6] are chosen to propagate the dynamics of the spacecraft. Compared to other element sets, such as the classical orbital elements or Cartesian coordinates, the MEEs present several advantages that make them well-suited for multi-revolution low-thrust trajectory optimization. The first five elements behave as slow variables, in contrast to Cartesian coordinates which are all fast variables. Slow variables are particularly attractive from a numerical standpoint as they remain in the linear domain for longer and thus increase the domain of convergence of the trajectory optimization problem. Furthermore, the MEEs are valid for circular, elliptic and hyperbolic trajectories, and they only suffer from singularities when the inclination is equal to $180°$, whereas the classical orbital elements encounter singularities when the eccentricity is 0 or when the inclination is either $0°$ or $180°$.

Equations of Motion

The MEEs (p,f,g,h,k,l) are related to the classical orbit elements (a,e,i,Ω,w,ν) through the following set of equations:

$$
\begin{aligned}
p &= a(1-e^2), & f &= e\cos(\Omega+w), & g &= e\sin(\Omega+w),\\
h &= \tan\left(\frac{i}{2}\right)\cos(\Omega), & k &= \tan\left(\frac{i}{2}\right)\sin(\Omega), & l &= \Omega+w+\nu,
\end{aligned}
$$

where a is the semimajor axis, e is the eccentricity, i is the inclination, Ω is the right ascension of the ascending node, w is the argument of perigee and ν is the true anomaly.

Let $\mathbf{x} = [p, f, g, h, k, l]^T$ denote the vector of MEEs and let $\mathbf{a} = [a_r, a_t, a_n]^T$ and $\mathbf{u} = [u_r, u_t, u_n]^T$ denote the vector of perturbing gravitational accelerations and the vector of thrust acceleration respectively, with components in the local-vertical/local-horizontal (LVLH) reference frame. The

dynamics of MEEs can be written as

$$\dot{\mathbf{x}} = \mathbf{A}(\mathbf{x}) + \mathbf{B}(\mathbf{x})\mathbf{a} + \mathbf{B}(\mathbf{x})\mathbf{u}, \tag{1}$$

where $\mathbf{A}(\mathbf{x})$ is given by

$$\mathbf{A}(\mathbf{x}) = \begin{bmatrix} 0 & 0 & 0 & 0 & 0 & \sqrt{\mu p}\left(\frac{q}{p}\right)^2 \end{bmatrix}^T, \tag{2}$$

$\mathbf{B}(\mathbf{x})$ is given by

$$\mathbf{B}(\mathbf{x}) = \begin{bmatrix} 0 & \frac{2p}{q}\sqrt{\frac{p}{\mu}} & 0 \\ \sqrt{\frac{p}{\mu}}\sin l & \sqrt{\frac{p}{\mu}}\frac{1}{q}[(q+1)\cos l + f] & -\sqrt{\frac{p}{\mu}}\frac{g}{q}[h\sin l - k\cos l] \\ -\sqrt{\frac{p}{\mu}}\cos l & \sqrt{\frac{p}{\mu}}\frac{1}{q}[(q+1)\sin l + g] & \sqrt{\frac{p}{\mu}}\frac{f}{q}[h\sin l - k\cos l] \\ 0 & 0 & \sqrt{\frac{p}{\mu}}\frac{s\cos l}{2q} \\ 0 & 0 & \sqrt{\frac{p}{\mu}}\frac{s\sin l}{2q} \\ 0 & 0 & \sqrt{\frac{p}{\mu}}\frac{1}{q}[h\sin l - k\cos l] \end{bmatrix}, \tag{3}$$

and $q = 1 + f\cos L + g\sin L$ and $s^2 = 1 + h^2 + k^2$.

The equations of motion, which include the variation of the mass, the control and the gravitational perturbations are written as

$$\dot{\mathbf{x}} = \mathbf{A} + \mathbf{B}\mathbf{a} + \frac{T\delta}{m}\mathbf{B}\hat{\mathbf{u}}, \tag{4}$$

$$\dot{m} = -\frac{T}{c}\delta, \tag{5}$$

In the above equations, m is the mass of the spacecraft, T is the maximum engine thrust, $0 \leq \delta \leq 1$ is the engine throttle, $c = I_{\text{sp}}g_0$ is the exhaust velocity, and $\hat{\mathbf{u}}$ is the control direction unit vector. I_{sp} and g_0 are the specific impulse and the gravitational acceleration at sea level.

Third-body Gravity Perturbations

In addition to the two-body gravitational effect caused by the Sun, our model includes the third-body perturbation exerted by the Earth and Mars. Modeling these perturbations is essential to generating realistic trajectories, because cycler orbits involve flybys at relatively close distance of the planets. In Cartesian coordinates, third-body perturbations are expressed as

$$\mathbf{t} = -\sum_{i=1}^{n}\mu_i\left(\frac{\mathbf{d}_i}{d_i^3} + \frac{\mathbf{s}_i}{s_i^3}\right) \tag{6}$$

By using Battin's formulation,[7] which reduces numerical errors, the above expression can be rewritten as

$$\mathbf{t} = -\sum_{i=1}^{n} \frac{\mu_i}{d_i^3}\left[\mathbf{r} + F(q_i)\mathbf{s}_i\right] \tag{7}$$

where

$$F(q_i) = q_i\left(\frac{3 + 3q_i + q_i^2}{1 + (\sqrt{1+q_i})^3}\right) \tag{8}$$

and

$$q_i = \frac{\mathbf{r}^T(\mathbf{r} - 2\mathbf{s_i})}{\mathbf{s}_i^T\mathbf{s}_i}. \tag{9}$$

Finally, the acceleration in the LVLH frame is given by

$$\mathbf{a}_t = \mathbf{Q}^T\mathbf{t} \tag{10}$$

where $\mathbf{Q}$ is the rotation matrix from the inertial frame to the LVLH frame, which is given by

$$\mathbf{Q} = \left[\begin{array}{ccc} \hat{\mathbf{i}}_r & \hat{\mathbf{i}}_t & \hat{\mathbf{i}}_n \end{array}\right] \tag{11}$$

with

$$\begin{aligned} \hat{\mathbf{i}}_r &= \frac{\mathbf{r}}{\|\mathbf{r}\|} \\ \hat{\mathbf{i}}_n &= \frac{\mathbf{r}\times\mathbf{v}}{\|\mathbf{r}\times\mathbf{v}\|} \\ \hat{\mathbf{i}}_t &= \mathbf{i}_n \times \mathbf{i}_r \end{aligned}$$

Minimum-Fuel Optimal Control Formulation

Considering a fixed time-of-flight, minimum fuel trajectories are found by minimizing the cost functional

$$J = \int_{t_0}^{t_f} \frac{T}{m(t)}\delta(t)\,dt, \tag{12}$$

which requires determining the optimal control policy $\delta(t)^*$ and $\hat{\mathbf{u}}^*$ within a set of admissible controls. The necessary condition of optimality for this problem is given by Pontryagin's Minimum Principle, which states that the optimal control policy must minimize the Hamiltonian of the system. The Hamiltonian is written as

$$H = \frac{T}{m}\delta + \boldsymbol{\lambda}^T\mathbf{A} + \boldsymbol{\lambda}^T\mathbf{B}\left(\frac{T}{m}\delta\hat{\mathbf{u}} + \mathbf{a}\right), \tag{13}$$

where $\boldsymbol{\lambda} = [\lambda_p, \lambda_f, \lambda_f, \lambda_h, \lambda_k, \lambda_l]^T$ is the vector of costates associated with the MEEs. The time derivatives of the costates are given by the Euler-Lagrange equations.

$$\dot{\boldsymbol{\lambda}} = -\left[\frac{\partial H}{\partial \mathbf{x}}\right]^T. \tag{14}$$

$$\tag{15}$$

The Hamiltonian is a linear function of both the thrust direction vector $\hat{\mathbf{u}}$ and the engine throttle magnitude δ. Thus, the optimal thrust direction $\hat{\mathbf{u}}^*$ that minimizes the Hamiltonian is obtained as

$$\hat{\mathbf{u}}^* = \frac{\mathbf{u}}{||\mathbf{u}||} = -\frac{\mathbf{B}^T\boldsymbol{\lambda}}{||\mathbf{B}^T\boldsymbol{\lambda}||}, \tag{16}$$

which is also known as Lawden's Primer vector.[8] Similarly, the optimal engine throttle δ required to minimize the Hamiltonian is computed as follows. Substituting $\hat{\mathbf{u}}$ from Eq. 16 into the Hamiltonian and collecting all terms that contain δ leads to the following expression that must be minimized.

$$-\frac{T}{m}\left(\left\|\mathbf{B}^T\boldsymbol{\lambda}\right\| - 1\right)\delta \rightarrow \min. \tag{17}$$

The terms inside the parenthesis are used to define a switching function

$$S \equiv \left\|\mathbf{B}^T\boldsymbol{\lambda}\right\| - 1. \tag{18}$$

Thus, the optimal value of the throttling input δ^* depends on the sign of the switch function S, which produces a *bang-bang* control profile

$$\delta^*(S) = \begin{cases} 1, & \text{if } S > 0, \\ 0, & \text{if } S < 0 \end{cases} = \frac{1}{2}\left[1 + \text{sign}(S)\right]. \tag{19}$$

In order to avoid sharp changes in the dynamics, which is challenging for numerical integrators and decreases the radius of convergence of the problem, the thrust profile is smoothed using a hyperbolic tangent function and continuation.[9,10]

TRAJECTORY DESIGN

In this section we investigate the use of solar electric propulsion (SEP) as a means to inject the courier (data mule spacecraft) into the Earth-Mars cycler orbit and to maintain the cycler orbit by targeting selected Earth and Mars flybys. Our aim is to design trajectories in the ephemeris model that minimize the amount of propellant required for injection and cycler maintenance while maximizing the amount of data that can be uplinked and downlinked during the respective Earth and Mars flybys. During our analysis we found that the amount of propellant required for insertion is much greater than that for maintaining the cycler orbit, and for now we have treated these as separate elements of the mission design process.

Assumptions

In our orbit simulations we have assumed a ESPA-compatible[11] spacecraft with a mass of 500 kg that is equipped with the NEXT ion engine.[12] We assume that the NEXT ion engine is operating in the most efficient mode, with a specific impulse of 4155 seconds and a thrust magnitude of 0.235 N. To meet our data transfer mission objective, we require that the Earth/Mars flybys occur at an altitude of no more than 25,000 km above the surface of each planet and impose lower bound altitude flyby constraints of 300 km and 1000 km for Mars and Earth respectively. We also assume that the low-thrust engine remains off during the flybys so that the data mule can achieve the attitude required to communicate with other spacecraft or ground stations. If thrusting was required during the flybys, the cycler spacecraft orientation would be determined by the thruster pointing requirements which would likely be sub-optimal for data transfer. Finally, we assume that the cycler spacecraft is launched as part of a rideshare with another Mars bound mission, and after separation it uses its own propulsion system to target Earth-Mars cycler orbit insertion (COI).

Methodology Overview

The trajectory design for this mission is divided into two parts. The goal for the first part is to find trajectories in a high-fidelity model that have repeated flybys of Earth and Mars with desired characteristics. Solutions to this complex problem are found by first solving a similar problem with lower-fidelity models and those results are then used to initialize the optimization with the higher-fidelity model. In the second part of the design, we solve for trajectories that depart from Earth and inject into the Earth-Mars cycler orbits. In particular, we are interested in rideshare transfers, which implies that the departure state near Earth is constrained by the trajectory of the primary mission. In both parts of the design, the high-fidelity low-thrust trajectories are found by solving an optimal control problem using the indirect approach described earlier in the paper. The state-costate equations are propagated using a Runge-Kutta 9(8) integrator, and the two-point boundary value problem (TPBVP) arising from the optimal control formulation is solved using Matlab's fsolve with a multiple-shooting method.

Cycler Injection

We assume that the cycler spacecraft are launched as a secondary payload (i.e. rideshare) on board a mission that is already bound for Mars. The main mission reaches Mars using a direct transfer, typically lasting about 7 months. These direct transfers are easily computed using a Lambert solver. Figure 2 shows the C3 contours for various departure times and transfer times (time-of-flight) for the direct transfer to Mars. The dashed red line indicates the time-of-flight of the transfer. Note the local minimum occurring in mid-June 2035 with a transfer time of about 190 days.

Once Mars bound, the data mules use their own onboard low-thrust propulsion system to target injection into a particular cycler orbit. The cycler orbit injection is formulated as an indirect optimal control problem that leads to a two-point boundary value problem that must be solved. The starting point of the low-thrust trajectory is computed by choosing a specific rideshare geometry for the main mission (departure epoch and arrival epoch), which determines the state vector at departure assuming two-body dynamics and no planetary bodies. This guess is further refined by computing the Earth parking orbit and escape hyperbola corresponding to the Lambert solution. The terminal boundary condition for the cycler orbit insertion is determined by searching through the database (see below) of precomputed cycler orbit trajectories for a Mars flyby that occurs at least 800 days after the departure from Earth. Since thrusting is not permitted during the planetary encounter, the target point is set at a distance of three times the size of the sphere of influence of Mars, so that the flyby is ballistic.

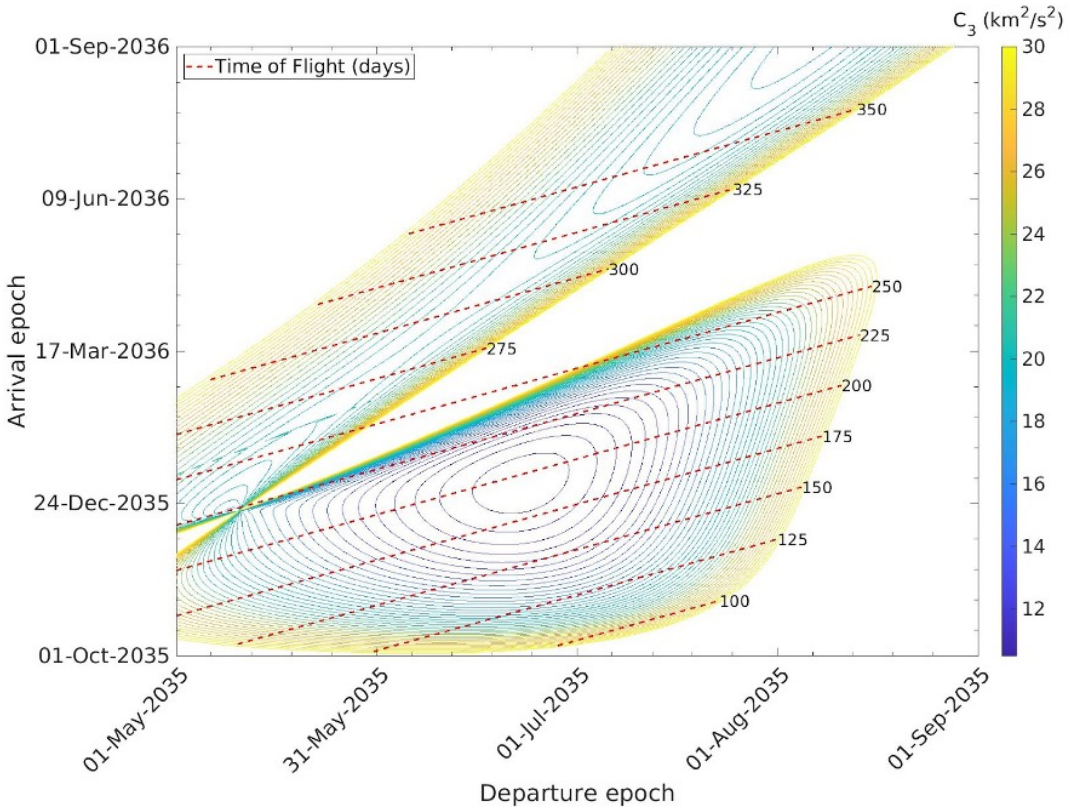

Figure 2. C3 contours for Earth to Mars trajectories with various departure and arrival epochs.

Cycler Orbiting and Targeting

The procedure used to obtain high-fidelity Earth-Mars cyclers is illustrated in detail in the following paragraphs. As noted in,[13] directly obtaining cycler orbits in an ephemeris model is often impractical if not impossible. Thus, the trajectory design is divided in five sub-problems that are solved sequentially, which simplifies the process of transitioning solutions to a higher fidelity model.

Step 1: Patched Conic Trajectories JPL's in-house STAR software[14] was used to generate thousands of Earth-Mars cycler trajectories with a patched conic model (Figure 3). These low-fidelity solutions can be generated quickly and allow the entire solution space to be sampled. This database of low-fidelity solutions was filtered to select trajectories that satisfied specific Δv and flyby altitude requirements as candidates for steps 2 through 4.

Step 2: Two-body Impulsive The entire set of solutions obtained in step 1 was then refined using a more realistic dynamical model. In the patched conic approximation, flybys are determined as instantaneous changes in the heliocentric velocity vector of the spacecraft, but no information is provided regarding the position vector of the spacecraft when it crosses the sphere of influence of the planet. Thus, a TPBVP was solved using two-body dynamics, to generate planetocentric flyby trajectories whose incoming and outgoing velocity vectors match those computed by STAR. These

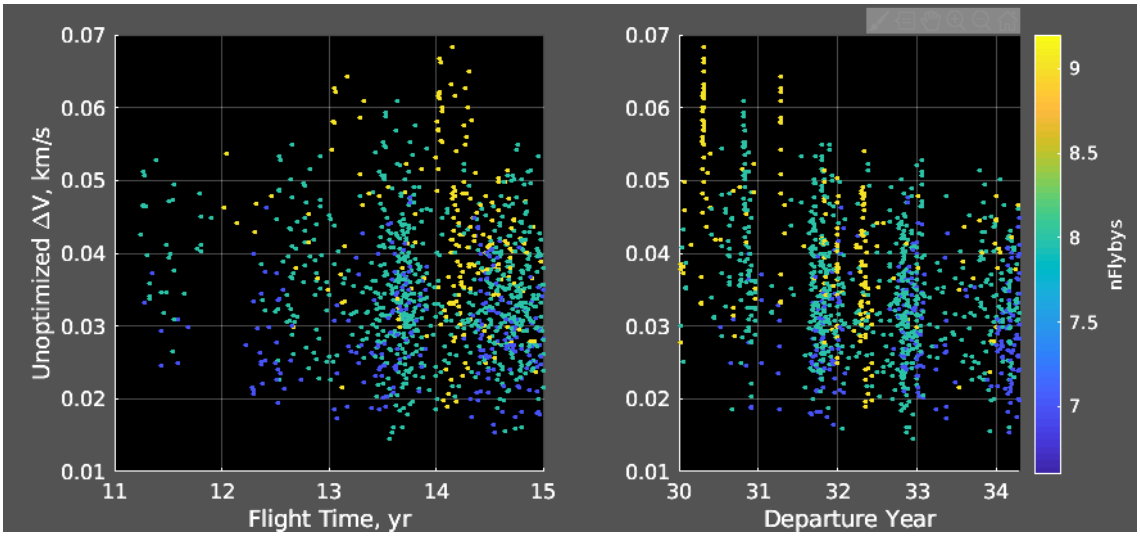

Figure 3. Full dataset returned by Star with Mars-Earth transit duration constrained to be shorter than 12 months.

two-body trajectories are easily computed, and the results match the properties of the original trajectories (incoming and outgoing velocity vectors, flyby altitude, flyby impulsive Δv) with negligible difference.

Step 3: Medium-fidelity Impulsive The converged solutions from step 2 were then used to initialize an impulsive trajectory optimization scheme that takes into account perturbations from other bodies in the solar system. We found that the Sun's gravity significantly perturbs the trajectory of the spacecraft during the planetary flybys and thus the incoming and outgoing vectors computed by STAR result in very large Δv's for the flyby targeting problem. To reduce the Δv we propagate the trajectory backward and forward from each flyby and solve for the trajectory that minimizes the mismatch in position and velocity at the heliocentric breakpoint (i.e. a point in interplanetary space, midway between the flybys). The propagation is done in the heliocentric frame and gravity perturbations from the planets are included in the dynamical model. This results in trajectory segments that are smooth in position and velocity everywhere except at the heliocentric breakpoints (Figure 4). These solutions were then fed to the low- thrust optimizer (step 4).

Step 4: High-fidelity Low-Thrust The solutions from step 3 were then used as an initial guess for solving the low-thrust optimal control problem, by essentially replacing the interplanetary trajectory mismatch (discussed in step 3) with optimally computed low-thrust arcs (Figure 5). The fuel-optimal trajectory is computed using an indirect optimal control formulation as described earlier in the paper. This approach results in a TPBVP and a switch function that determines the time and duration of thrust and coast arcs. We found that the high-fidelity impulsive solutions are a very good initial guess for the low-thrust optimal control problem, however the run-time is significantly longer than that required in the previous steps. As a result, it was not possible to converge the entire STAR dataset of low-thrust cycler spacecraft in the ephemeris model. However, we have converged several and discuss one candidate solution in detail in the following section.

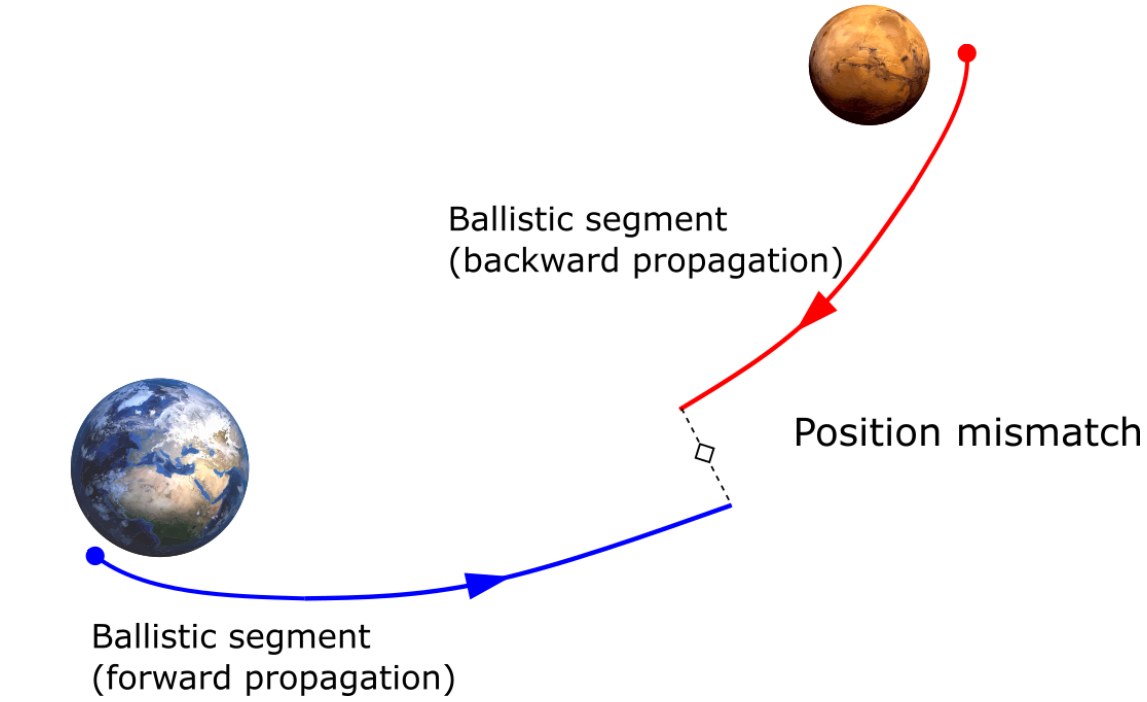

Figure 4. Impulsive trajectory optimization between flybys to minimize the mismatch at the break point.

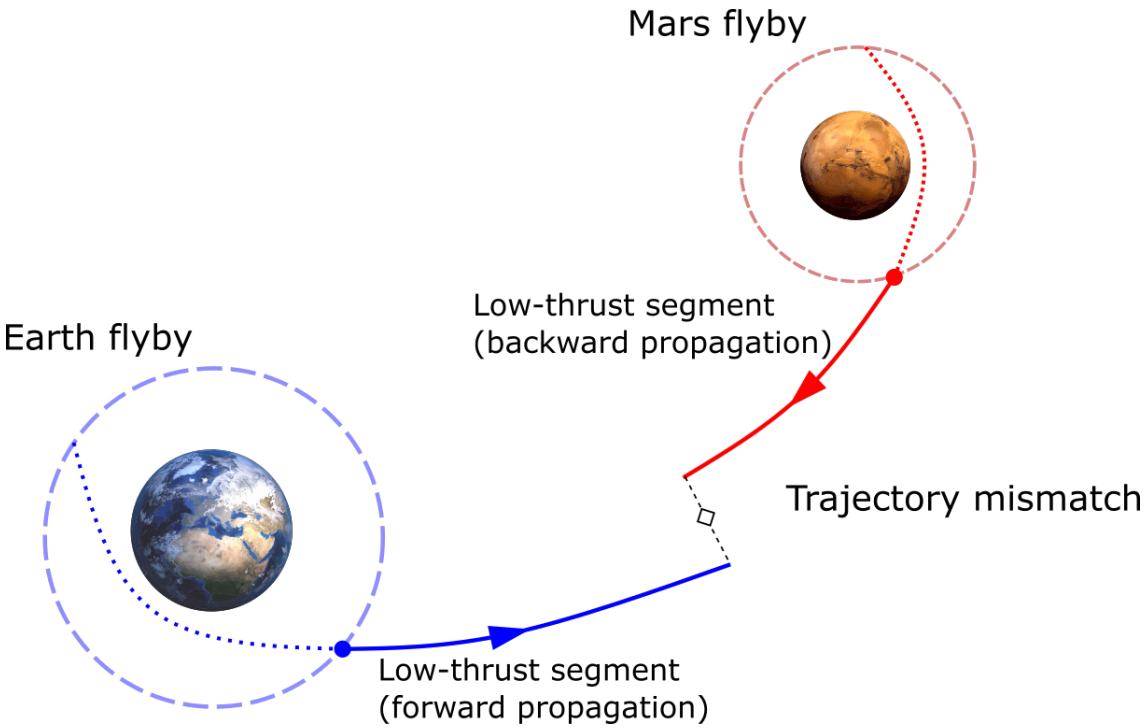

Figure 5. Low-thrust trajectory optimization between flybys to replace the impulsive Δv with optimally placed low-thrust arcs.

Step 5: Polynomial Thrust-arc Fitting The fuel-optimal low-thrust trajectory obtained in step 4 is then post-processed to obtain precise times for the thruster on/off switches. The procedure in step 4 makes use of a continuation parameter that smooths the on/off control switches to improve convergence. In certain situations where the Δv is very small, this can lead to solutions with long thrust arcs where thrust magnitude is much lower than the prescribed value. These numerical artifacts are easily overcome by fitting the thrust control time history with a polynomial and iterating on the values of the polynomial coefficients and the duration of the thrust arc such that the problem boundary conditions are still met. This post-processing step converges rapidly and yields a solution with negligible difference in fuel consumption, compared with step 4, but gives precise thruster on/off times which are necessary for mission operations.

RESULTS

Following the steps above, we were able to converge 278 of STAR's patched conic trajectories in the ephemeris model using impulsive thrust (i.e. up to step 3), and several trajectories all the way through step 5. Our investigation revealed that most of the propellant budget is required for COI, and once the spacecraft is on the cycler orbit a minimal amount of fuel (< 5 kg) is needed to maintain the orbit and target flybys. In this paper we present and discuss the results for one of the fully converged solutions that spans from mid-2037 to the beginning of 2046, and only required 36 kg of propellant for the entire mission. For better visual clarity, the solutions for the injection and targeting phases are shown on different figures.

Figure 6 shows the trajectory of the rideshare mission (pink), along with the data mule's optimal low-thrust COI trajectory (blue) and the respective orbits of the Earth (green) and Mars (red). Figure 7 shows the control profile and spacecraft mass as a function of the mission time. For this particular COI solution, four thrust arcs are require with thrust durations of weeks to months. This COI phase requires the bulk of the total propellant budget for the mission. Figures 8 through 12 show the flyby targeting portion of the mission. Figures 8, 9, and 10 show the same cycler orbit in the patched conics (step 1), impulsive (step 3) and low-thrust (step 5) models respectively. It is evident that while the direction of the thrust vector changes, the trajectory does not vary significantly. Figure 11 shows the difference between the patched conics solution and the low-thrust solution as a function of mission duration. Finally, Figure 12 shows the control profile and mass history as a function of time for the flyby targeting phase of the mission. The for this particular solution the thrust arcs last between 10 and 20 hours only about 2 kg of propellant is required.

Figure 13 shows the data crosslink for an example cycler orbit trajectory. The top panel shows the distance between the data mule and observer spacecraft orbiting Mars. The middle panel shows the supportable optical crosslink data rate in Mbps for the given distance. The bottom panel shows the cumulative data volume transferred between the observer and the data mule during the crosslink in Tbits. The data rate is adjusted as the relative distance between the spacecraft decreases, thus maximizing the data transfer between the two vehicles. As is evident in the figure, the total data volume returned during the 8 flybys (> 8000 Tbits) exceeds our goal of returning, on average, about 1 Petabit per year. More details on the crosslink analysis are given in.[5,15]

FUTURE WORK

The minimal amount of propellant required for cycler orbit targeting in the ephemeris model opens the door to considering even smaller and cheaper classes spacecraft. As mentioned previously, the bulk of the propellant mass for the mission was needed for the COI. Other technology such as

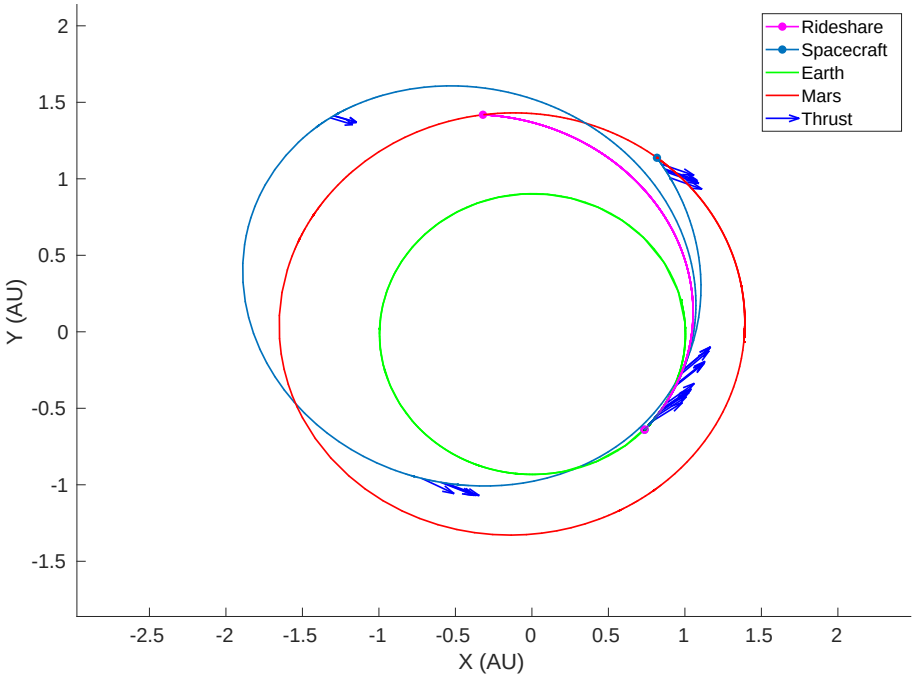

Figure 6. Cycler Orbit Injection Trajectory

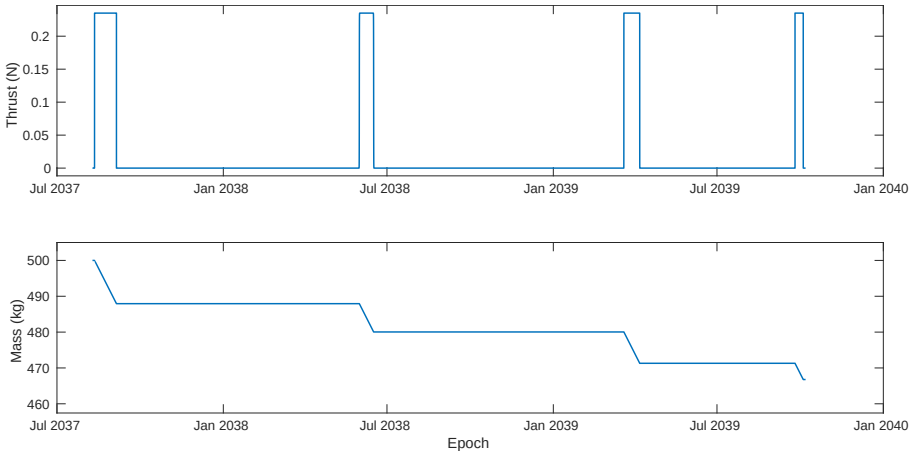

Figure 7. Injection thrust profile and mass consumption.

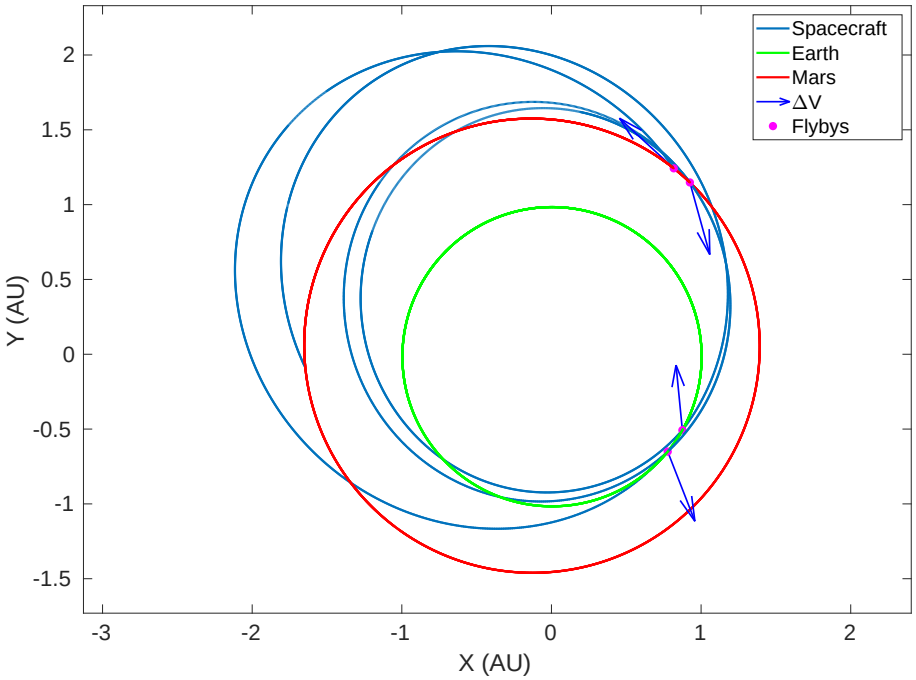

Figure 8. Solution obtained using patched conics (STAR)

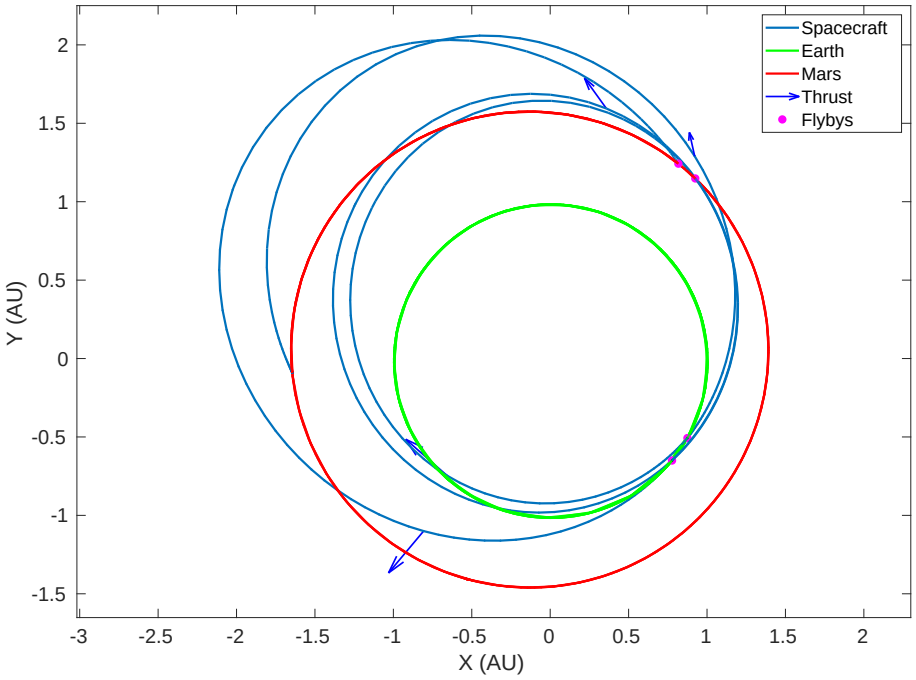

Figure 9. Solution obtained using impulsive thrust and ephemeris model.

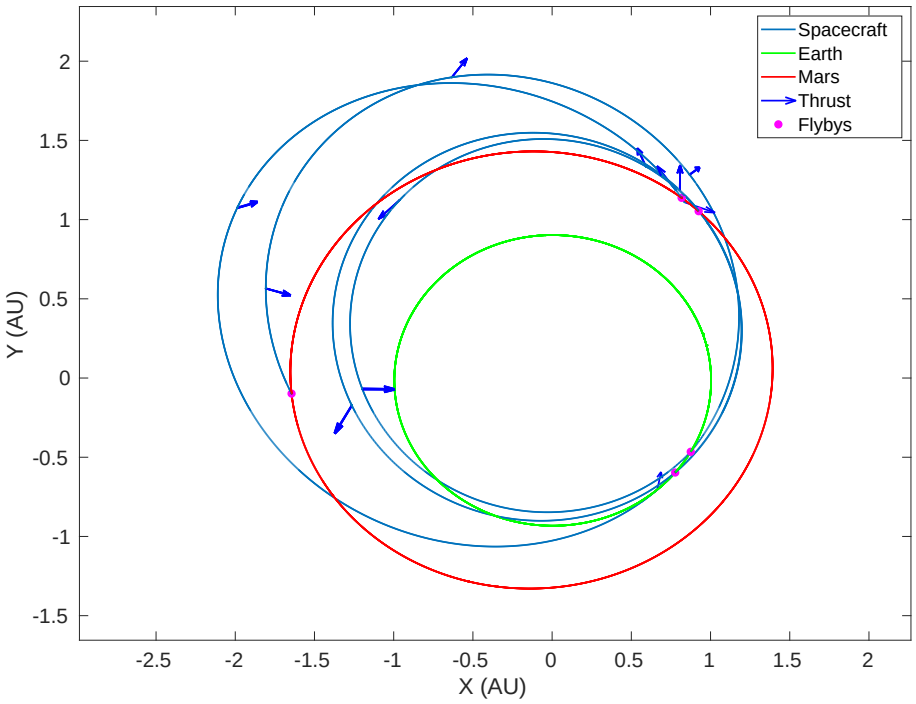

Figure 10. Solution obtained using low-thrust and ephemeris model.

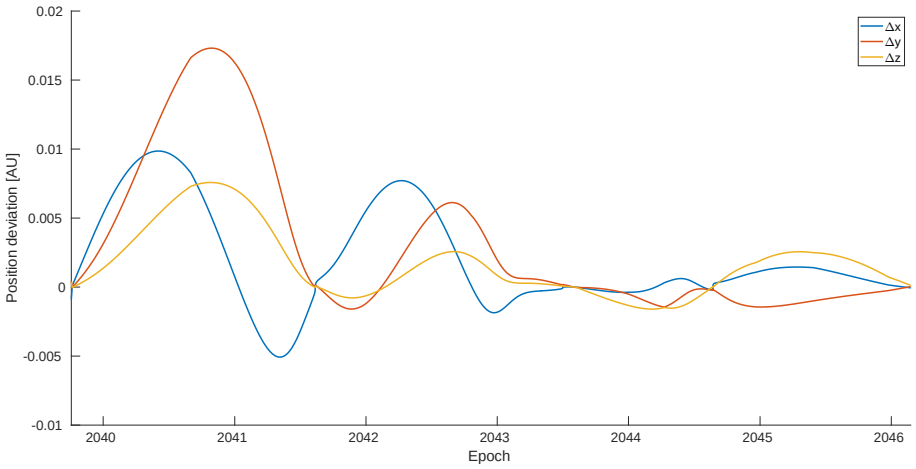

Figure 11. Deviation between patched conics and low-thrust trajectories.

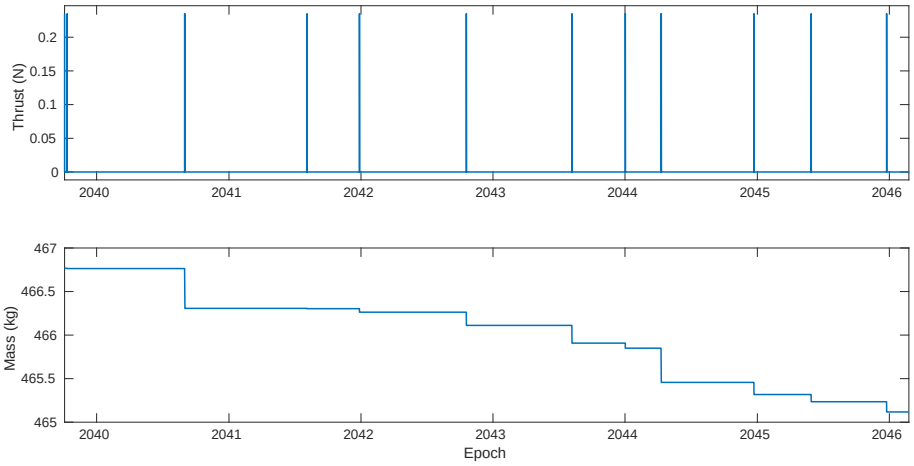

Figure 12. Thrust profile and mass consumption for the low-thrust solution in the ephemeris model.

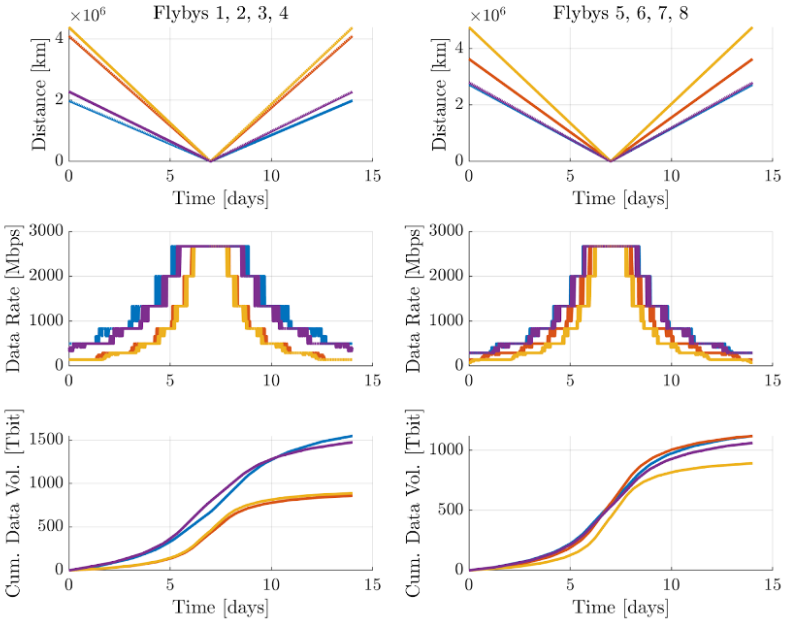

Figure 13. Cross link analysis

using a space tug to inject multiple smaller spacecraft (i.e. 100 kg) into the cycler orbit would eliminate the need for a large on board COI propulsion system, thus further reducing the size of the cycler spacecraft. A smaller propulsion system, such as the MiXi low-thrust engine, may be a good candidate for consideration in future work. In addition to investigating different mission architectures, we also intend to improve the efficiency of the optimization procedure in order to more quickly converge low-thrust trajectories using the high-fidelity ephemeris model.

CONCLUSION

We have developed a method for designing and optimizing Earth-Mars cycler trajectories for the Solar System Pony Express (SSPE). For this mission concept, courier satellites are launched as a rideshare payload with another Mars-bound mission. Each courier flying in the SSPE network is equipped with a low-thrust propulsion system that is used for cycler orbit injection and for targeting the flybys of Earth and Mars. Cycler orbits are first computed using a patched conic approximation and impulsive thrust. These candidates are then transitioned into a higher-fidelity ephemeris model and fuel-optimal, low-thrust, transfers are solved between each pair of flybys, using an indirect optimization method. We presented a high-fidelity solution where a 500 kg courier spacecraft is inserted into an Earth-Mars cycler using only 36 kg of propellant, and a further 2 kg of propellant is required to target eight subsequent flybys over a period of six years. This is very feasible from a mission design perspective and it also demonstrates that solutions obtained in the patched conics model can be successfully transitioned to the ephemeris model using low-thrust propulsion.

ACKNOWLEDGMENT

The research was carried out at the Jet Propulsion Laboratory, California Institute of Technology, and at the University of Illinois at Urbana-Champaign, under a contract with the National Aeronautics and Space Administration. This work was funded by the NASA NIAC Program (80NM0018D0004).

REFERENCES

[1] M. S. Net, E. Pellegrini, and J. V. Hook, "Cycler Orbits and the Solar System Pony Express," *2020 IEEE Aerospace Conference*, IEEE, Mar. 2020, 10.1109/aero47225.2020.9172342.

[2] H. Hemmati and D. Caplan, "Chapter 4 - Optical Satellite Communications," *Optical Fiber Telecommunications (Sixth Edition)* (I. P. Kaminow, T. Li, and A. E. Willner, eds.), Optics and Photonics, pp. 121–162, Boston: Academic Press, sixth edition ed., 2013, https://doi.org/10.1016/B978-0-12-396960-6.00004-3.

[3] D. V. Byrnes, J. M. Longuski, and B. Aldrin, "Cycler orbit between Earth and Mars," *Journal of Spacecraft and Rockets*, Vol. 30, May 1993, pp. 334–336, 10.2514/3.25519.

[4] W. M. Hollister and M. D. Menning, "Periodic swing-by orbits between earth and Venus," *Journal of Spacecraft and Rockets*, Vol. 7, Oct. 1970, pp. 1193–1199, 10.2514/3.30134.

[5] M. S. Net, E. Pellegrini, W. Parker, and J. V. Hook, "Solar System Data Mules: Analysis for Mars and Jupiter," *2021 IEEE Aerospace Conference (50100)*, 2021, pp. 1–8, 10.1109/AERO50100.2021.9438463.

[6] M. J. H. Walker, B. Ireland, and J. Owens, "A set modified equinoctial orbit elements," *Celestial Mechanics*, Vol. 36, Aug. 1985, pp. 409–419, 10.1007/bf01227493.

[7] R. Battin, *An Introduction to the Mathematics and Methods of Astrodynamics*. AIAA Education Series, 1999.

[8] D. F. Lawden, *Optimal trajectories for space navigation*. Butterworths, 1963, chp.3.

[9] E. Taheri and J. L. Junkins, "Generic Smoothing for Optimal Bang-Off-Bang Spacecraft Maneuvers," *Journal of Guidance, Control, and Dynamics*, Vol. 41, No. 11, 2018, pp. 2470–2475.

[10] R. M. Woollands, E. Taheri, and J. L. Junkins, "Efficient Computation of Optimal Low Thrust Gravity Perturbed Orbit Transfers," *The Journal of the Astronautical Sciences*, Vol. 67, No. 2, 2019, pp. 458–484, 10.1007/s40295-019-00152-9.

[11] J. R. Maly, S. A. Haskett, P. S. Wilke, E. Fowler, D. Sciulli, and T. E. Meink, "ESPA: EELV Secondary Payload Adapter with whole-spacecraft isolation for primary and secondary payloads," *Smart Structures and Materials 2000: Damping and Isolation*, Vol. 3989, International Society for Optics and Photonics, 2000, pp. 430–439.

[12] J. Fisher, "NEXT-C Flight Ion System Status," *AIAA Propulsion and Energy 2020 Forum*, American Institute of Aeronautics and Astronautics, August 2020, 10.2514/6.2020-3604.

[13] R. P. Russell and C. A. Ocampo, "Optimization of a Broad Class of Ephemeris Model Earth-Mars Cyclers," *Journal of Guidance, Control, and Dynamics*, Vol. 29, Mar. 2006, pp. 354–367, 10.2514/1.13652.

[14] D. Landau, S. Campagnola, and E. Pellegrini, "Star Searches for Patched-Conic Trajectories," *The Journal of the Astronautical Sciences*, 2022 (submitted).

[15] M. S. Net, E. Pellegrini, W. Parker, J. V. Hook, and R. Woollands, "Small Satellites on Cycler Orbits with Optical Communication Enable Regular High Volume Data Transfer from Mars," *Joural of Spacecraft and Rockets*, 2022.